Generating High-Brightness Electron Beams via Ionization Injection by Transverse Colliding Lasers in a Plasma-Wakefield Accelerator

F. Li,[1] J. F. Hua,[1] X. L. Xu,[1] C. J. Zhang,[1] L. X. Yan,[1] Y. C. Du,[1] W. H. Huang,[1] H. B. Chen,[1] C. X. Tang,[1] W. Lu,[1,2,*] C. Joshi,[2] W. B. Mori,[2] and Y. Q. Gu[3]

[1]*Key Laboratory of Particle and Radiation Imaging of Ministry of Education, Tsinghua University, Beijing 100084, China*
[2]*University of California Los Angeles, Los Angeles, California 90095, USA*
[3]*Laser Fusion Research Center, China Academy of Engineering Physics, Mianyang, Sichuan 621900, China*

(Received 14 January 2013; published 2 July 2013)

The production of ultrabright electron bunches using ionization injection triggered by two transversely colliding laser pulses inside a beam-driven plasma wake is examined via three-dimensional particle-in-cell simulations. The relatively low intensity lasers are polarized along the wake axis and overlap with the wake for a very short time. The result is that the residual momentum of the ionized electrons in the transverse plane of the wake is reduced, and the injection is localized along the propagation axis of the wake. This minimizes both the initial thermal emittance and the emittance growth due to transverse phase mixing. Simulations show that ultrashort (~ 8 fs) high-current (0.4 kA) electron bunches with a normalized emittance of 8.5 and 6 nm in the two planes, respectively, and a brightness of 1.7×10^{19} A rad^{-2} m^{-2} can be obtained for realistic parameters.

DOI: 10.1103/PhysRevLett.111.015003 PACS numbers: 52.38.Kd, 41.75.Jv, 52.35.Mw

The demonstration of the Linac Coherent Light Source (LCLS) as an x-ray free electron laser (X-FEL) [1] has given impetus to research on fifth-generation light sources [2]. The goal is smaller and cheaper X-FELs with shorter wavelengths and increased coherence and intensity. The FEL performance is partially determined by the brightness of the electron beam that traverses the undulator, which is defined as $B_n = 2I/\epsilon_n^2$ where I and ϵ_n are the beam current and normalized emittance, respectively. To drive the SASE-FEL [3] into saturation with much shorter undulator, high-current ($\sim$ kA) multi-GeV electron beams with $\epsilon_n \sim 10$ nm will be needed. These emittances are an order of magnitude smaller than those from state-of-the-art photoinjector rf guns [4]. In this Letter, we show the generation of ultrabright electron bunches using ionization injection triggered by two transversely overlapping laser pulses inside a beam-driven wake in plasma. The relatively low intensity lasers are polarized along the wake axis and overlap with the wake for a very short time. Three-dimensional particle-in-cell (PIC) simulations using OSIRIS [5] show that this geometry reduces the residual momentum of the ionized electrons in the transverse plane and localizes them along the propagation axis of the wake leading to an electron beam with a normalized emittance of 8.5 and 6 nm in the two planes, respectively, and a brightness of 1.7×10^{19} A rad^{-2} m^{-2}, which is three orders of magnitude brighter than that of the electron beams driving LCLS.

When a dense ($n_b > n_p$, $k_p \sigma_{r,z} < 1$), ultrarelativistic ($\gamma \gg 1$) electron beam propagates through a plasma, the plasma electrons can be completely blown out by the beam's Coulomb force leaving behind a cavity of more massive ions [6–8] which then pull the electrons back creating a wakefield with a phase velocity equal to the beam's velocity. Here, n_b, n_p, k_p, and $\sigma_{r,z}$ are beam density, plasma density, inverse of the plasma skin depth, and transverse and longitudinal rms size of the electron beam, respectively. The accelerating and focusing fields inside this wakefield have ideal properties for acceleration of electrons while maintaining beam quality [6–8], and high-gradient acceleration by such wakes has been experimentally demonstrated [9–12].

For a plasma density $\sim 10^{18}$ cm^{-3}, the ion cavity wavelength is about several tens of microns making the synchronization and efficient capture of externally injected electrons into such a cavity extremely challenging. Self-injection of electrons in plasma wakes is conceptually simple; however, it still cannot generate sufficiently high brightness beams needed for next-generation light sources [13,14]. Other electron injection schemes, such as ponderomotive force injection [15], injection via external magnetic field [16], and collinear colliding pulse injection [17], were proposed and the latter was experimentally demonstrated [18]. In addition, a sudden [19] or gradual [20] density transition from a high plasma density to a low plasma density has also been shown to inject particles into plasma wakes. Another technique is ionization injection where electrons are produced inside the wake by the electric field of a laser pulse or the drive electron beam where they can be more easily captured and accelerated. Ionization injection is attractive because it offers the potential to control the accelerated beam's charge and emittance. Very recently it was proposed to combine the ionization injection via an auxiliary laser pulse into a beam-driven wake [21]. This approach allows the use of a lower intensity ionizing laser, thereby further reducing the injected electron's transverse emittance. In this Letter,

we show that electron injection into a beam-driven plasma-wakefield accelerator via tunnel ionization in the overlap region of two laser pulses (moving transversely across the wake) can generate an electron beam with extremely small transverse emittances and therefore extremely high brightnesses.

This mechanism is explored using the 3D PIC code OSIRIS [5] in Cartesian coordinates using a moving window. We define the z axis to be the drive beam's propagating direction, and the x axis to be the colliding laser pulses' propagating direction with their electric field polarized along the z axis. The simulation window has a dimension of $89 \times 81 \times 121$ μm with $1400 \times 512 \times 760$ cells in the x, y, and z directions, respectively. This corresponds to cell sizes of $0.5k_0^{-1}$ in the x direction and $1.25k_0^{-1}$ in the y and z directions. The code uses the Ammosov-Delone-Krainov tunneling ionization model [22].

For simplicity, the simulation is initialized with plasma with a density of $n_p = 2.4 \times 10^{17}$ cm^{-3} represented by 8 particles per cell, and neutral He with a density of 1.1×10^{18} cm^{-3} represented by 8 neutral atoms per cell. The preionized plasma can be viewed as a fully ionized separate gas. A 500 MeV drive beam with $n_b = [N/(2\pi)^{3/2}\sigma_z\sigma_r^2]e^{-r^2/2\sigma_r^2}e^{-z^2/2\sigma_z^2}$ propagates through the plasma and excites the wake, where $\sigma_z = 11.4$ μm, $\sigma_r = 7.6$ μm, and the total electron number $N = 1.25 \times 10^9$ (200 pC). The beam's self-electric field (~ 50 GeV/m) does not ionize the helium atoms. In addition, two counter-propagating laser pulses moving along the $+$ and $-$ x-axis directions are synchronized with the electron beam so that they overlap inside the ion cavity near the point where the longitudinal electric field E_z vanishes. Each laser has a normalized vector potential $a_0 = 0.016$, a duration $\tau = 20$ fs, and a focal spot size $w_0 = 6\,\mu$m. These parameters correspond to each laser having a focused intensity of 5.5×10^{14} W/cm^2 for a wavelength of 800 nm.

We first examine the injection process. It is easier to trap and to control the self-injection of an electron that is born (ionized) at rest inside the wake. The trapping threshold is given by [23] $\Delta\psi \equiv \psi - \psi_{\rm init} < -1 + (1 + [p_\perp/mc]^2)^{1/2}/\gamma_{\rm ph}$ where $\psi \equiv e(\phi - A_z)/mc^2$ is the normalized wake potential, and $\psi_{\rm init}$ is the wake potential when and where an electron is created. The wake potential is a minimum at the rear of the ion cavity, so it is easiest to trap an electron born where the potential is a maximum ($E_z = 0$) which occurs in the middle of the cavity. Furthermore, low emittance beams are generated if the electrons are born near the wake axis. For laser ionization, the electron is born inside the laser, so it acquires a residual drift of $p/mc = eA_{\rm init}/mc^2$ in the direction of $A_{\rm init}$. The amount of injected charge is proportional to the neutral gas density.

Figure 1 illustrates the proposed injection process. In Fig. 1(a) , the injector laser pulses are just moving across the sharp electron sheath of the ion cavity. Because the laser pulse(s) intensity is low $\sim 5.5 \times 10^{14}$ W/cm^2, the ponderomotive force of the lasers does not perturb the sheath electrons. In Fig. 1(b), the lasers collide on the wake axis, where they have the maximum (overlapping) intensity at the position where $E_z = 0$. The laser intensity exceeds the ionization threshold only where the lasers overlap (each laser intensity is below the ionization threshold), and a large fraction of neutral helium atoms within this volume is now ionized. As the lasers travel past the collision point, the injection ceases. The drift momentum of the electrons is along the laser polarization direction and therefore affects predominantly the longitudinal momentum spread of the beam, leading to a longitudinal emittance of 0.06 keV ps in this example. These laser-ionized helium electrons then respond to the wake fields and are rapidly accelerated to a longitudinal velocity close to c as they slip backwards to the rear of the ion cavity. They then begin to move nearly synchronously with the wake, as depicted in Fig. 1(c).

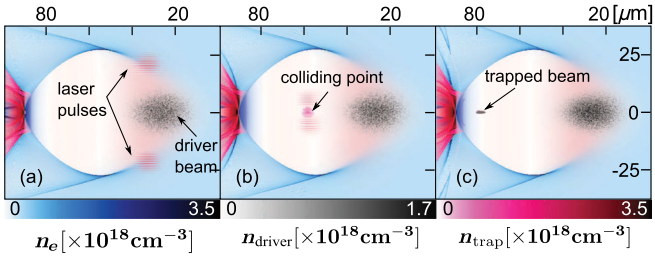

FIG. 1 (color online). Snapshots (a)–(c) show the charge density distribution of driver beam, wake electrons, and helium electrons at three different times. Here the densities of the drive electron beam, wakefield electrons, and field-ionized electrons are plotted respectively. (a) $\sim$80 fs before laser pulses collision, (b) around the laser pulses' collision time, (c) $\sim$200 fs after collision when the injected electrons become trapped in the wake. The ionized electrons seen on the left of each figure are from the wakefields exceeding the ionization threshold for helium at the rear of the cavity; none are accelerated in the wakefield.

More details are seen by plotting the density of the He^+ ions. The superposition of the two lasers gives rise to a standing wave with an intensity 4 times that of a single pulse and a node spacing of $\lambda_0/2$. Figure 2 shows the He^+ ion density resulting from laser ionization at two times. The laser created He^+ ions are immobile; thus, their location represents the birthplace of the electrons. In Fig. 2(a), one can observe the layered ion density reflecting the standing wave of the electric field at the instant where the lasers overlap. In Fig. 2(c), a lineout corresponding to the red dashed line of Fig. 2(a) is shown. The inset shows that He atoms are almost fully ionized to He^+ at the antinodes of the overlapping intensity. Helium electrons are mainly born within 2 μm of the axis. In Fig. 2(b) we show a snapshot of ion density 80 fs after the laser collision when the lasers are near the sheath. The superposition of the laser and wakefields near the electron sheath leads to some off-axis ionization. Additionally, there is ionization

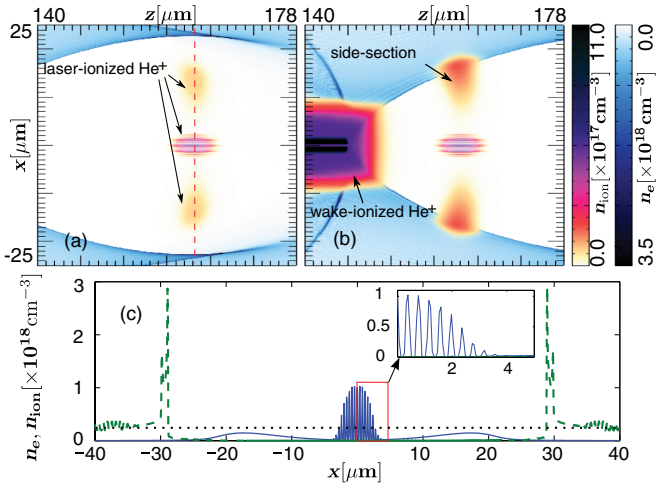

FIG. 2 (color online). Ion density indicates the ionization level of helium gas. (a) Ionization level at the instant of collision. (b) 80 fs after the collision when the lasers are on the verge of exiting the wake. (c) The lineout on the dashed line in (a). Laser-ionized He^+ are shown with solid line, sheath electron density with dashed line, and dotted line indicates the initial ion background.

from the wakefield alone near the rear of the bubble. Fortunately, in this case these off-axis electrons (and those in the rear) are lost because their initial positions are too close to the rear and too far from the axis of the cavity.

Figure 3 shows the phase space in each plane ~500 fs after the collision. The projected normalized emittance $\epsilon_n = \overline{\beta\gamma}\sqrt{\langle x'^2\rangle\langle x^2\rangle - \langle xx'\rangle^2}$ is calculated for each of the two transverse planes. Initially, the injected beam has an ultralow projected transverse ϵ_n for the whole bunch of about 8.5 nm in the x direction and 6 nm in the y direction, which is observed to be invariant after propagating 100 μm. At this distance, the beam has an average energy 5.3 MeV, with a rms correlated energy spread (chirp) of 0.2 MeV, a slice energy spread of ~12 keV, and a total charge of 4.6 pC. The beam current profile is near flattop, with a rms pulse duration around 8 fs and peak current 0.44 kA. The brightness B_n is 1.7×10^{19} A rad^{-2} m^{-2}, more than 3 orders of magnitude higher than that of LCLS. The total energy spread of the bunch can be reduced further by optimizing beam loading [24,25] and further acceleration by a longer wavelength wake.

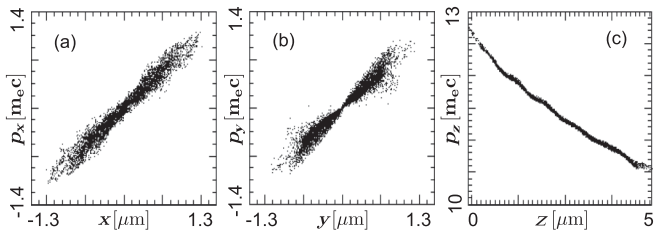

FIG. 3. The (a) x-p_x, (b) y-p_y, and (c) z-p_z phase space distribution about 500 fs after the pulse collision.

To achieve extremely small ϵ_n, conditions have to be fulfilled. First, electrons have to "start" with small transverse momenta. In the proposed scheme, since the laser pulses are polarized along the z axis and propagate perpendicularly to the x axis, the electric field components E_x, E_y, E_z scale as $E_x \sim \epsilon E_z$, $E_y \sim \epsilon^2 E_z$, where ϵ is a characteristic small parameter defined as $\epsilon \equiv 1/k_0 w_0$, around 0.02 in our simulation; therefore, the residual transverse momenta p_x, p_y of electrons just after ionization scale as $p_x/m_e c \sim \epsilon a_0$, $p_y/m_e c \sim \epsilon^2 a_0$, which are extremely small. Second, the transverse electron beam sizes w_b are determined by the laser intensity contour above the ionization threshold near the collision point, approximately $w_b \propto c\tau$, which for the simulated parameters is around a few microns. Combining these two factors, the intrinsic or "thermal" emittance of the electron beam, which is defined as $\epsilon_{\rm th} = \langle p_\perp \rangle w_b$, is very small. The use of two intense transversely propagating lasers was recently proposed for laser-driven wakes [26]; however, a beam driver ionizes the plasma to a much lower degree than an intense laser driver due to its much lower self-field, so injection laser pulses with much lower intensity can be used to trigger further ionization leading to beams with much smaller emittance.

However, to preserve the "thermal" emittance, it is necessary to avoid phase mixing, which arises when electrons are born at different times and therefore at different phases of their betatron oscillations. To illustrate this point, we simulate the injection process of both the transverse colliding pulse injection scheme (this Letter) and the recently proposed longitudinal injection scheme [21]. In the longitudinal injection scheme, a single injection laser pulse propagates collinearly at an optimum distance (67 fs) behind the beam driver, where $E_z = 0$. For both simulations, the drive beam is the same, with 200 pC of charge and $\sigma_r = \sigma_z = 3.8$ μm, and the preionized plasma density is set to 5×10^{17} cm^{-3}. The simulation domain is 63.5 μm $\times$ 50.8 μm $\times$ 63.5 μm and $1000 \times 400 \times 500$ cells were used in the transverse injection case and $500 \times 400 \times 1000$ cells in the longitudinal injection case. The injection lasers have the same pulse duration ($\tau = 20$ fs) and a FWHM spot size (5 μm) but with different focal intensities. For longitudinal injection, the laser is polarized in the x direction and focused with $a_0 = 0.035$ or an intensity of 2.6×10^{15} W/cm^2. For the colliding pulse injection, each laser has a $a_0 = 0.016$; therefore, near the antinode of the standing wave, the combined laser intensity is just above the ionization threshold of helium. The neutral helium densities are also different, 1.1×10^{18} cm^{-3}, and 5.2×10^{16} cm^{-3} for the "transverse" and "longitudinal" propagation cases, respectively. By doing so, both cases yield similar injected charge (1.9 pC for transverse injection and 3 pC for longitudinal injection). For higher helium density in the longitudinal injection case, the injected charge can be larger but the emittance gets much worse; e.g., for the same He density as that used in the

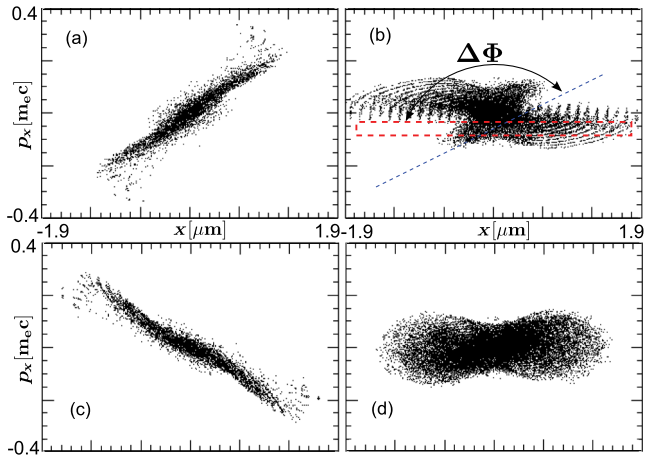

FIG. 4 (color online). Comparison of x-p_x phase space evolution between the transverse colliding pulses injection (a),(c) and the longitudinal injection (b),(d) at 130 fs (a),(b) and 260 fs (c),(d) after the onset of injection.

transverse injection case, ϵ_n was 10 times worse. We also have simulated the colliding pulse geometry with the lasers polarized along y instead of z. In this case, the thermal emittance along y is comparable to that of the longitudinal case illustrating the importance of minimizing both the thermal emittance and phase mixing.

Figure 4 illustrates that the x-p_x phase space evolution is very different between the transverse colliding pulses injection (left column) and the longitudinal injection (right column). Figures 4(a) and 4(b) are taken 130 fs after the onset of injection (at this time, injection has ceased for colliding pulses while it is still ongoing for the longitudinal injection scheme). Figures 4(c) and 4(d) are taken about 260 fs after the onset of injection. There is phase space rotation in the colliding pulse case (as expected), and there is far less phase space mixing as compared to longitudinal injection because the injection distance in the longitudinal scheme is much longer than that in the colliding pulse scheme. The injection distance in the longitudinal case is on the same order as the Rayleigh length of the laser pulse, $z_R = \pi w_0^2/\lambda_0$. Over this distance, He electrons born at different times have different betatron [27] phase Φ in both transverse directions. We define $\Delta\Phi$ as the betatron phase difference between the first and the last ionized electron. As seen in Fig. 4(b), the first ionized electrons have rotated to the blue dashed line, while the final ionized electrons have just been released (roughly in the dashed box). A longer injection distance will cause a larger $\Delta\Phi$, thereby leading to a larger final emittance. The effect of phase mixing is much reduced in the proposed scheme because all the He electrons are released in a short time controlled by the overlap time of the lasers. As shown in Figs. 4(a) and 4(c), the electrons rotate in phase space with a small phase divergence. In simulations, the normalized emittances in the longitudinal injection scheme are 34 nm

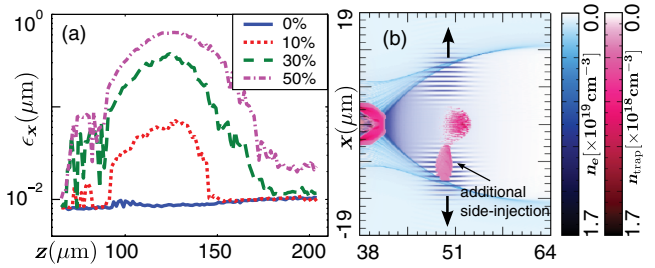

FIG. 5 (color online). The impact of laser power imbalance on ϵ_n. (a) Variation of ϵ_n during the trapping process under different laser power mismatch ratios. (b) Additional helium electrons generated on the higher power side for the 30% power mismatch.

in the x direction and 25 nm in the y direction, both 4 times larger than those obtained in the transverse colliding pulses injection scheme.

The issues of possible concern are time jitter (between the laser pulses <1 fs, between lasers and the beam—presently <100 fs but likely to improve to <10 fs), pointing accuracy (better than a few μrad), and power imbalance. Here we examine the effect of power imbalance between the two colliding laser pulses. Assuming the total power is fixed, we define the power mismatch ratio $R = 1 - P_L/P_H$, where P_L, P_H represent the lower and higher laser power, respectively. We use simulation parameters identical to those of Fig. 4(a) and the results are shown in Fig. 5.

In Fig. 5(a), the evolution of $\epsilon_{n,x}$ starting from the birth of helium electrons is plotted. Except for the $R = 1$ case, all other curves rise rapidly first and then eventually drop to a low level. This reduction can be understood from Fig. 5(b). After the collision is over, a large number of additional helium electrons are liberated in the wake by the overlapping of the higher power laser and the wake fields. These electrons lead to emittance growth because they are born with transverse positions far off axis. However, the majority of these additional electrons do not get trapped ($\Delta\Psi > -1$) and fall behind leading to the drop in the emittance over time. The final emittance can be as low as 10 nm as long as the power mismatch is less than 30% and with approximately the same charge.

This work was supported by NSFC Grants No. 11175102 and No. 11005063, Tsinghua University Initiative Scientific Research Program, the Thousand Young Talents Program, DOE Grants No. DE-FG02-92-ER40727, No. DE-SC0008491, and No. DE-SC0008316, and NSF Grants No. PHY-0936266 and No. PHY-0960344. Our simulations used the Hoffman and Dawson2 Clusters at UCLA.

*weilu@tsinghua.edu.cn

[1] P. Emma *et al.*, Nat. Photonics **4**, 641 (2010).
[2] C. Pellegrini, in *Workshop on 5th Generation Light Sources* (Catalina, California, October 7–12, 2010).

[3] M. J. Hogan *et al.*, Phys. Rev. Lett. **81**, 4867 (1998).
[4] C. G. Limborg-Deprey *et al.*, SLAC Report No. SLAC-PUB-14692, 2012.
[5] R. A. Fonseca *et al.*, *Computational Science ICCS 2002* (Springer, Berlin, 2002), Vol. 2331, pp. 342–351.
[6] J. B. Rosenzweig, B. Breizman, T. Katsouleas, and J. J. Su, Phys. Rev. A **44**, R6189 (1991).
[7] W. Lu, C. Huang, M. Zhou, W. B. Mori, and T. Katsouleas, Phys. Rev. Lett. **96**, 165002 (2006).
[8] W. Lu, C. Huang, M. Zhou, M. Tzoufras, F. S. Tsung, W. B. Mori, and T. Katsouleas, Phys. Plasmas **13**, 056709 (2006).
[9] C. Joshi *et al.*, Phys. Plasmas **9**, 1845 (2002).
[10] P. Muggli *et al.*, Phys. Rev. Lett. **93**, 014802 (2004).
[11] M. J. Hogan *et al.*, Phys. Rev. Lett. **95**, 054802 (2005).
[12] I. Blumenfeld *et al.*, Nature (London) **445**, 741 (2007).
[13] G. R. Plateau *et al.*, Phys. Rev. Lett. **109**, 064802 (2012).
[14] S. M. Wiggins *et al.*, Plasma Phys. Controlled Fusion **52**, 124032 (2010).
[15] D. Umstadter, J. K. Kim, and E. Dodd, Phys. Rev. Lett. **76**, 2073 (1996).
[16] J. Vieira, S. F. Martins, V. B. Pathak, R. A. Fonseca, W. B. Mori, and L. O. Silva, Phys. Rev. Lett. **106**, 225001 (2011).
[17] E. Esarey, R. F. Hubbard, W. P. Leemans, A. Ting, and P. Sprangle, Phys. Rev. Lett. **79**, 2682 (1997).
[18] J. Faure, C. Rechatin, A. Norlin, A. Lifschitz, Y. Glinec, and V. Malka, Nature (London) **444**, 737 (2006).
[19] H. Suk, N. Barov, J. B. Rosenzweig, and E. Esarey, Phys. Rev. Lett. **86**, 1011 (2001).
[20] C. G. R. Geddes, K. Nakamura, G. Plateau, Cs. Toth, E. Cormier-Michel, E. Esarey, C. Schroeder, J. Cary, and W. Leemans, Phys. Rev. Lett. **100**, 215004 (2008).
[21] B. Hidding, G. Pretzler, J. B. Rosenzweig, T. Königstein, D. Schiller, and D. L. Bruhwiler, Phys. Rev. Lett. **108**, 035001 (2012).
[22] M. V. Ammosov, N. B. Delone, and V. P. Krainov, Sov. Phys. JETP **64**, 1191 (1986).
[23] A. Pak, K. A. Marsh, S. F. Martins, W. Lu, W. B. Mori, and C. Joshi, Phys. Rev. Lett. **104**, 025003 (2010).
[24] M. Tzoufras, W. Lu, F. Tsung, C. Huang, W. Mori, T. Katsouleas, J. Vieira, R. Fonseca, and L. Silva, Phys. Rev. Lett. **101**, 145002 (2008).
[25] M. Tzoufras, W. Lu, F. S. Tsung, C. Huang, W. B. Mori, T. Katsouleas, J. Vieira, R. A. Fonseca, and L. O. Silva, Phys. Plasmas **16**, 056705 (2009).
[26] M. Chen *et al.*, AIP Conf. Proc. **1507**, 262 (2012).
[27] S. Wang *et al.*, Phys. Rev. Lett. **88**, 135004 (2002).